Available online at www.sciencedirect.com

ScienceDirect

Energy Procedia 00 (2018) 000–000

Energy Procedia

www.elsevier.com/locate/procedia

16th International Symposium on District Heating and Cooling, DHC2018,
9–12 September 2018, Hamburg, Germany

Thermal and hydraulic investigation of large-scale solar collector field

Nirendra Lal Shrestha[a*], Ophelia Frotscher[a], Thorsten Urbaneck[a], Thomas Oppelt[a], Thomas Göschel[b], Ulf Uhlig[b], Holger Frey[b]

[a]*Chemnitz University of Technology, Faculty of Mechanical Engineering, Professorship Tehnical Thermodynamics, 09107 Chemnitz, Germany*
[b]*inetz gmbH, Augustusburger Straße 1, 09111 Chemnitz, Germany*

Abstract

Large collector fields are increasingly being integrated into district heating systems. Due to the operation mode of these networks, the solar system must provide the desired supply temperature. Therefore, knowledge of thermal-hydraulic behavior and energy efficiency are very important for planning, operation and control. The study presents the investigation of two large-scale solar collector fields in Chemnitz (Germany). For the detailed study of heat transfer and hydraulic behavior of the field, mobile monitoring has been installed on selected rows in addition to the conventional monitoring system. The measurement results show that large collector fields with differently sized rows, consisting of a large number of collectors with a dividing manifold (below) and a combining manifold (above) connected to a large row, can be operated with a variable flow rate (matched flow). With the provided measured values, comparison of the desired/actual values and the calculation of absolute and relative parameters are performed. The Brühl solar district heating system has been in operation since summer 2016 and meets the expectations of thermal performance and efficiencies.

Keywords: collector; field; solar thermal system; monitoring; efficiency; hydraulic; performance; operation; measurement

* Corresponding author. Tel.: +49 37153132637; fax: +49 371531832637.
E-mail address: nirendra-lal.shrestha@mb.tu-chemnitz.de

Nomenclature

a_0	conversion factor, -	FM	flow meter
a_1	linear heat loss coefficient, W/(K·m^2)	g	global radiation
a_2	quadratic heat loss coefficient, W/(K^2·m^2)	in	inlet
c	specific heat capacity, kJ/(kg·K)	m	mean
f_O	safety factor for other uncertainties, -	max	maximum
f_P	safety factor taking into account heat loss from pipes, -	meas	measured value
f_U	safety factor taking into account measurement uncertainty, -	min	minimum
		N	row in the north field
G	global radiation, W/m^2	NF	north field
H	daily global radiation, kWh/m^2	nom	nominal
p	pressure, Pa	Pa	sensor, ambient pressure
Q	thermal energy, kWh	r	return
$\dot{Q}$	thermal power, kW	rad	radiation
T	temperature, °C, K	s	supply
$\dot{v}$	specific flow rate, l/(m^2·h)	S	row in the south field
$\dot{V}$	flow rate, m^3/h	SF	south field
η	efficiency, -	SHCT45	Solar Heating and Cooling Task 45
ρ	density, kg/m^3	Ta	sensor, ambient temperature
a	ambient	TC	thermocouple
cm	combining manifold	Trad1	sensor, outside temperature with influence of sky radiation
coll	collector		
diag	diagonal	Trad2	sensor, outside temperature with influence of ground radiation
dm	dividing manifold		
Ecoll	sensor, solar radiation on collector surface	w	water
Fa	sensor, outside air humidity	Ww	sensor, wind velocity

1. Introduction

From 2011 to 2014, the Professorship Technical Thermodynamics at the Chemnitz University of Technology and the *inetz* company (district heating operator) developed a highly efficient district heating system with solar thermal system and combined heat and power for the urban quarter Brühl in Chemnitz (Germany) considering of complex urban development conditions [1], [2], [3]. The system was built between 2015 and 2016. In summer 2016, the solar plant was put into operation. The monitoring and analysis are carried out as part of the project "Solar district heating for the Brühl district in Chemnitz – accompanying research (SolFW)" which is located in the 6th energy research program of the German federal government [1].

This article refers to the operation of large collector fields. The collector field operated with variable flow should provide heat at the desired supply temperature[1]. The heat can then be directly fed into the network or used for charging the storage. For reliable operation, it is necessary to know the thermal and hydraulic conditions. In the system presented here, the questions are not trivial, as there is an irregular structure of the fields (in contrast to [5]). Moreover, many large collectors are connected in parallel. From practice, there are only a few results available [5, 6]. In this article, the energy efficiency of the collector fields is also considered together with the thermal-hydraulic behavior (for e.g. collector's efficiency, thermal power output).

[1] The first known large-scale plant is located in Marstal (Denmark) [4]. There, this type of operation mode has been practiced since 1996 using large-scale collectors with harp absorbers by Arcon (12.5 m²).

2. Collector fields layout

The structure of the south and north solar collector field (ground-mounted) is shown in Fig. 1. Large-sized flat plate collectors from Wagner Solar [7] were used. The collector fields (Table 1) differ in number and length of the rows and in number and type of collectors installed. In order to ensure an optimal use of the field, two different sizes of collectors were installed in the system (WGK 80 and WGK 133 with three and five meander pipes, respectively). Each field is part of a collector circuit with independent operation. Each row (Fig. 2) consists of parallel-connected collectors, which have a common dividing and combining manifold. That means, each row forms an additional mesh system with the meanders in the collectors (Tichelmann circuit). Here is a difference to large-sized flat plate collectors which are internally fitted with harp absorbers. These collectors have been installed in the Danish large plants since the 1990s and each row consists of a series of harps. The sum of the pressure losses of all the collectors in the row gives the pressure loss of a row.

The operation of the system with variable flow rates (Table 1) should ensure an adjustable supply temperature (70…80 °C). Therefore, the rows are hydraulically balanced with regulating valves.

The special feature of the Brühl solar system [2], [3] is that water is used as heat transfer medium throughout the system. This means that no heat exchangers are used between the collector and the consumer. As a result, the following advantages can be achieved: improvement of the heat transfer in the collector and the venting, reduction of the temperature losses along the supply line, thereby increasing the collector output and yield, simplification of the safety technology. On the other hand, there are disadvantages of active frost protection, which are associated with low-temperature heat consumption and complex operation. In order to be able to evaluate this concept, first of all the thermal-hydraulic behavior and the operating results must be analyzed.

The measurement of the parameters of the plant is carried out by the project partner *inetz* through the conventional monitoring system. In addition, for the detailed measurement of the parameters to determine heat transfer and hydraulic behavior of the plant, mobile monitoring is installed in both fields (Fig. 2). Here, two rows (S6, S7, N5 and N6) with different numbers of collectors (Table 2) are fitted with the corresponding measuring equipment in both fields. The temperature sensors (Thermocouples, TC) were mounted at various positions on the dividing and combining manifolds[2] as well as on the absorber plate. The flowmeters were installed in the return pipes. Furthermore, environmental sensors were installed. The recording of the measurement is done for every minute, ensuring a high resolution of dynamic processes.

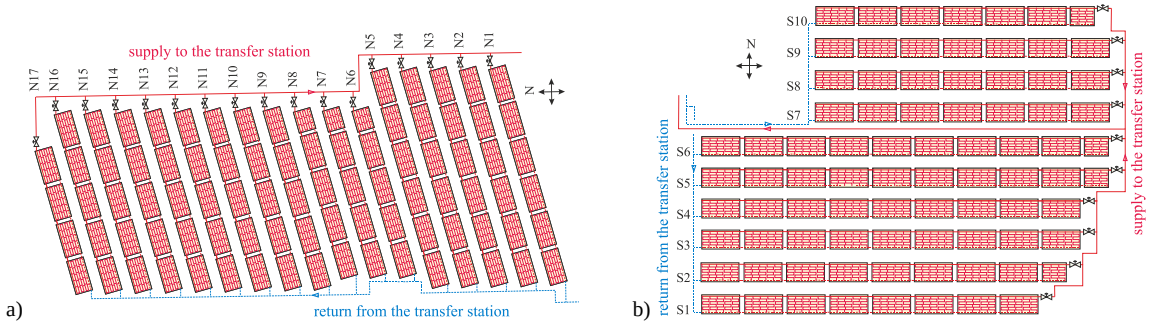

Fig. 1. Layout of the Brühl solar collector fields (a) north field; (b) south field.

[2] The mean collector temperature ($T_{m,coll,diag}$) is determined by averaging the temperature in the dividing and combining manifolds according to Fig. 2. Due to the surface temperature sensors, the heat transfer at the pipes influences the measurement of the heat transfer fluid's temperature. If the flow distribution in all the meander pipes in row is equal, then the temperature differences also match. The determination of the mean collector temperature is then relatively accurate. In the case of non-uniform temperature distributions in the meanders, deviations occur and the mean temperature ($T_{m,coll,diag}$) deviates from the actual mean value.

3. Analysis of the hydraulic behavior

3.1. Flow distribution and pressure loss in row

Fig. 3 shows the flow distribution in the meander pipes for the rows S6, S7, N5 and N6. The crosses represent the calculated flow rates in the meander pipes, respectively and the dashed line represents the desired flow rate with a uniform distribution. The maximum deviation occurs always in the last meander pipe. The flow distribution takes a parabolic form. The meander pipes in the center of the row have always the lowest flow rate. Despite the approximately parabolic distribution, the flow rate in the first meander do not reach the same values as those at the end of the row. This asymmetry results from the influences of the T-pieces. There are dividing and combining flows in the manifolds.

In row S6 (Fig. 3, red), the meanders 14 to 34 have an almost identical flow rate. Due to the low flow rates, the flow regimes lie in the transition region from turbulent to laminar flow. Therefore, the pressure losses are low and such a plateau is formed. The series connection of the collectors and the flow rate in the row also provides different pressure losses (Table 3). The deviation of the pressure losses in the meander pipes is also shown in Table 3.

Table 1. Parameters of the collector fields and specification of the operating range of the fields (matched flow), specific flow rate.

Parameter	North field	South field
Aperture area [m^2], fields	1086.08	1006.91
Aperture area, [m^2], total	2092.99	
No. of WGK 133AR/80AR [-]	86/3	79/4
No. of rows [-]	17	10
Interconnection of the rows	Parallel	
	No further subdivision	Additionally subdivided into two meshes
Min. / max. number of meander pipes per	20/30	33/48
Collector row distance [m]	3.74	
Collector tilt angle [°]	35	
Field azimuth [°]	-30	0
$\dot{v}_{nom.}$ [l/(m^2·h)]	15.00	
$\dot{v}_{min.}$ / $\dot{v}_{max.}$ [l/(m^2·h)]	11.12/23.00	9.03/24.80

Table 2. Parameters of the investigated rows with mobile monitoring.

Parameter	N5	N6	S6	S7
Aperture area [m^2]	74.22	56.90	118.75	86.59
Number of collectors WGK 13 /WGK 80	6/0	4/1	9/1	7/0
Number of meanders	30	23	48	35

3.2. Temperature distribution in row

A higher/lower flow rate means a lower/higher supply temperature during operation at nominal conditions. In the mobile monitoring, the temperatures in the combining manifolds T_{cm} and in the distributing manifolds T_{dm} (Fig. 2) are measured in the rows S6, S7, N5 and N6. The following diagrams in Fig. 4 depict the mean collector temperature and the mean temperature in row (line). The row S6 with the highest number of collectors (10 collectors, 48 meander pipes) shows approximately a parabolic shape. The collector temperature is in a range of 3 K (minimum measured value 62.75 °C, maximum measured value 65.78 °C). The temperature increase in the first four collectors is approximately linear. The seventh collector has the highest mean temperature. Then, temperature decreases again. The mirrored behavior of the temperatures in row (Fig. 4 a) indicates that the calculated flow distribution for the row S6 is correct at least qualitatively.

Row S7 (Fig. 4 b) depicts a similar temperature distribution as of the row S6, whereby the difference between the minimum and maximum values being only 1.43 K. This effect can be attributed to a more uniform flow distribution (Fig. 3), which results from a lower number of meanders.

The rows N5 and N6 (Fig. 4 c, d) show a small temperature deviation over the row. The lowest value occurs in the first collector. However, in row N6, the mean collector temperature in collector 5 does not drop. It must be remembered that the number of five collectors or measuring points is not adequate for a statement about the temperature behavior over the entire row with 23 meander pipes.

The tendency of the temperature curves nevertheless supports the calculation results of the flow rates, as the temperature is indirectly proportional to the flow rate. In addition, the deviation from the mean value increases both in the calculation of the flow rates and also in the observation of the mean collectors temperature. From this it can be concluded that the flow distribution is more uniform with a small number of meander pipes. However, the construction of large rows with up to 119 m^2 area can also be approved from a technical point of view.

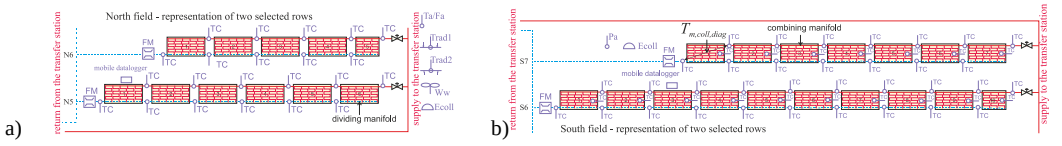

Fig. 2. Schematic representation of the mobile monitoring in the (a) north field and (b) south field.

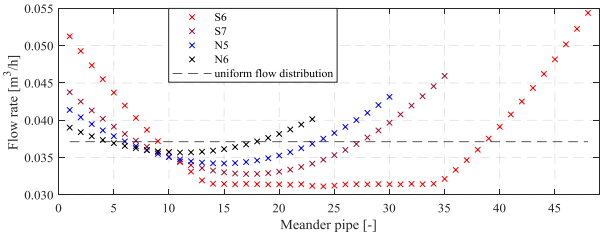

Fig. 3. Calculated flow rate per meander pipe for the rows S6, S7, N5 and N6 in comparison to a uniform flow distribution for nominal conditions with 15 l/(m^2·h).

Table 3. Calculated pressure losses for the rows with nominal conditions of 15 (l/m^2·h), fluctuations of pressure losses in the meander pipes.

	N5	N6	S6	S7
Pressure loss [mbar]	103.65	77.86	226.04	129.30
Min./max. deviation [%]	-8.2/+17.0	-4.1/+8.6	-15.9/+43.5	-12.2/+24.9

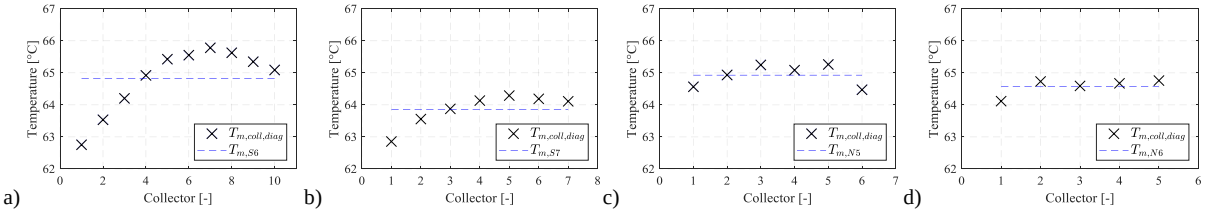

Fig. 4. Mean collector temperature for a) S6, b) S7, c) N5 and d) N6, averaging in the time 12:00 – 13:00, test day 15.10.2017.

3.3. Flow distribution and pressure loss in the field

The calculation of the pressure losses is very crucial for the design of a field. The pressure loss of a row depends strongly on the row length and the flow distribution (Fig. 5). Due to this reason, the flow distributions and pressure losses for an increased and reduced flow rate are calculated (Fig. 5). The maximum flow rate in both collector fields is approx. 25 m^3/h. During operation the flow rate is controlled accordingly within a range of 30 to 167 % of the nominal flow rate (15 l/(m^2·h)). As expected, the pressure losses increase with the increase of flow rates (Fig. 5). Also the deviations of the flow rates in the meander pipes increase (Fig. 6). However, the distribution of flow rates at

167 % is much more unfavorable than at 100 %[3]. In order to reach the desired supply temperature, the balancing valves are set for a flow distribution with 15 l/(m²·h). Due to the effects above presented, the operation should be kept as far as possible within the design range.

The flow distribution in the collector fields after hydronic balancing and with uniform flow distribution are shown in Fig. 7. The distribution in the north field shows a typical behavior, as described by *Eismann* [8]. The flow rate is higher than the average value in the rows which are close to the entrance of the return line in the field. Then the flow rate drops further. This explains the influence of the different row lengths and the associated pressure losses. In row N8, the calculated flow rate is higher than that of a uniform distribution. In row N9, both values are approximately the same. Subsequently, the calculated flow rates are below the values for a uniform distribution. In row N16, the difference between the two values is higher than in row N17. The distribution in the south field indicates a noticeable difference between the two sub-meshes of rows S1 to S6 with eight to ten collectors and S7 to S10 with seven collectors. Therefore, the flow rates of the rows S7 to S10 are above the desired values and rows S1 to S6 are below. Table 4 depicts the pressure loss in the fields and the maximum deviations of the pressure loss in a row to the respective uniform flow.

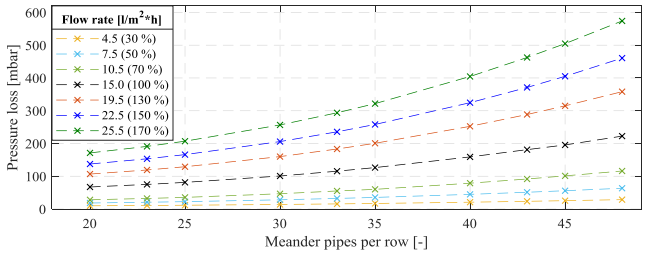

Fig. 5. Pressure losses over the row's length as a function of the specific flow rate and the number of meander pipes.

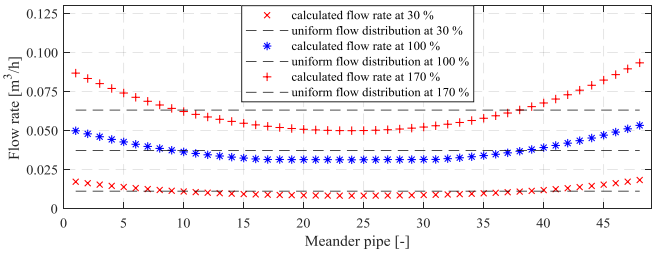

Fig. 6. Calculated flow distribution through the meanders in row S6 at a flow rate of 30 % 4.5 l/(m²·h), 100 % 15 l/(m²·h) and 170 % 25.5 l/(m²·h) as well as representation of the average values.

Fig. 8 illustrates the trend of the specific flow rates for each field and both the investigated rows after the hydronic balancing. In this case the specific flow rate of the field should be the desired value (blue). The measured specific flow rate in row S7 (yellow) is significantly higher than that of the field (Fig. 8 b). In contrast, the specific flow rate in row S6 (orange) is very close to the desired value. In the north field (Fig. 8 a), the deviation is relatively small for both rows. Table 5 depicts the maximum deviations of the rows to the respective desired values.

However, by evaluating the flow rate from the mobile monitoring, clear deviations were found in rows N5, N6 and S7 even at 15 l/(m²·h) (Fig. 8).

Row S6 is the first row starting from the entry of the return flow into the field (Fig. 1). Despite the high length of the row, the flow rate is identical to the planning values. This is because of the good setting of the valves. Row S7 is in a sub-mesh including the short rows S7-S10. Row S7 has the shortest connection to the supply and return line

[3] In this case, there is also an asymmetrical distribution due to the pressure loss coefficient of the T-pieces. The form of the flow distribution changes from the parabolic shape (30 %) via the parabola with plateau (100 %) to reformation of the parabolic form (170 %).

(Fig. 1). The short row length and the proximity to the field inlet enable the increased flow rate of the row[4]. An insufficient setting of the balancing valve at the supply line of the row is also responsible for this higher flow rate.

Rows N5 and N6 are connected directly one after the other. They differ significantly in their length. The pressure loss occurs mainly in the rows. This explains the marginal increase of flow in row N6.

The measurements are by no means contradictory to the hydraulic calculation. It must be checked whether a fine-adjustment of the balancing valves leads to an improvement of the flow distribution. If the field planning permits, the use of long rows near the field entrance is expected to be favorable.

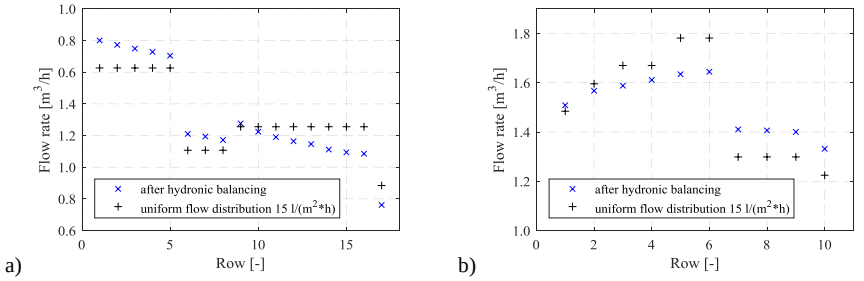

Fig. 7. Flow distribution in pressure balance and with uniform distribution in (a) north field and (b) south field.

Table 4. Pressure loss in the collector field and maximum deviation of the pressure loss in a row referred to a uniform flow distribution.

	North field	South field
Pressure loss [mbar]	123.17	199.04
Max. deviation [%], positive / row	7.54 / N1	8.85 / S10
Max. deviation [%], negative / row	8.85 / N16	7.97 / S5

Table 5. Specific flow rate of the row, deviation referred to a uniform flow distribution.

	N5	N6	S6	S7
Max. deviation [l/(m²·h)], absolute/relative value	-0.58/-3.7	+0.43/+2.7	±0.21/±1.2	+1.72/+10.2

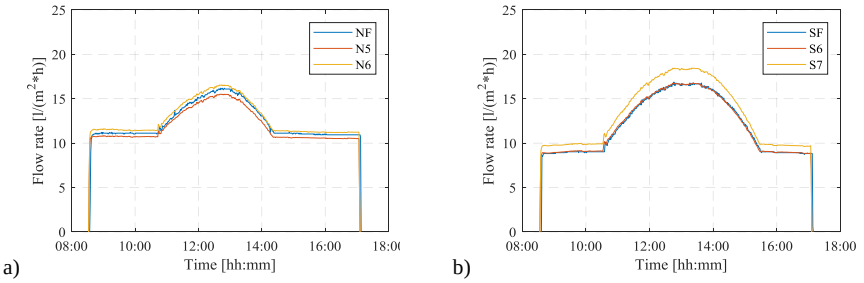

Fig. 8. Specific flow rate, measured values for (a) the north field and rows N5 and N6, (b) the south field and rows S6 and S7, test day 15.10.17.

4. Field thermal performance

4.1. Basic principles

The thermal power output of a collector is determined according to Eq. 1. Density and specific heat capacity of the water are characteristic properties and are dependent on the temperature.

[4] Other studies have shown that with the rows of equal length, the first row has a higher flow.

$$\dot{Q}_{coll} = \rho_W \dot{V}_{coll} c_{p,W} (T_{coll,out} - T_{coll,in}) \quad (1)$$

Capacitive effects of the collector and the heat transfer fluid (water) are neglected in this investigation. Therefore, quasi-stationary conditions are applied to all the analysis in this paper. Eq. 1 can also be applied to rows and fields [9]. So, additional heat losses for e.g. pipes are included.

The collector efficiency function is given by Eq. 2. It incorporates the parameters from the collector test. Therefore, this value is to be understood as a desired value. This equation can also be applied to a field or the particular rows. Then the field or the row is assumed to behave like the collector under test. In the mobile monitoring, the temperatures in the rows (N5, N6, S6 and S7) and the global solar irradiation on collector plane are determined. These measurements give a second interesting possibility for calculating the desired value as defined by Eq. 3. The averaged collector efficiency is determined by Eq. 2.

$$\eta_{coll,cal} = a_0 - a_1 \frac{(T_{coll,m} - T_a)}{G_{g,coll}} - a_2 \frac{(T_{coll,m} - T_a)^2}{G_{g,coll}} \quad (2)$$

$$\dot{Q}_{coll,S/N} = G_{g,coll,N/S} A_{coll,N/S} \eta_{coll,m} (T_{coll,m,N/S}) \quad (3)$$

The thermal power output according to Eq. 1 (actual value) can be used for measuring efficiency[5] (Eq. 4). The denominator represents available irradiation.

$$\eta_{coll,meas} = \frac{\dot{Q}_{coll}}{\dot{Q}_{rad}} = \frac{\rho_W \dot{V}_{coll} c_{p,W} (T_{coll,out} - T_{coll,in})}{A_{coll} G_{g,coll}} \quad (4)$$

Since the energy transport processes are very complex and fields are constructed differently, within the IEA SHC Task 45 [10], *Nielsen* and *Daniel* have developed a method to calculate the guaranteed power output (Eq. 5) of large solar systems. Analogous to Eq. 4, the solar radiation and the temperature difference to the ambient are incorporated. In addition, however, there are various safety factors which take into account the real boundary conditions (e.g. heat losses of the pipes, measurement uncertainties). The determination of the power output (Eq. 5) is based on the definition of efficiency (Eq. 2). Analogous to Eq. 4, the efficiency of the field can be calculated by Eq. 6.

$$\dot{Q}_{SHCT45} = A_{coll} \left[a_0 G_g - a_1 (T_m - T_a) - a_2 (T_m - T_a)^2 \right] f_P f_U f_o \quad (5)$$

$$\eta_{coll,SHCT45} = \frac{\dot{Q}_{SHCT45}}{\dot{Q}_{rad}} \quad (6)$$

The collector parameters required here were determined by TÜV Rheinland in accordance with EN 12975 and are listed in Table 6 [11]. Table 6 also contains the safety factors.

Table 6. Collector parameter from the collector test and safety factors according to the calculation procedure, IEA SHC Task 45.

a_0 [-]	a_1 [W/(m²·K)]	a_2 [W/(m²·K²)]	f_P [-]	f_U [-]	f_O [−]
0.857	3.083	0.013	0.970	0.900	0.950

4.2. Field thermal power output and collector efficiency

Fig. 9 illustrates the thermal power output (red), the supply and return temperatures (green/blue) of the fields and the field flow rate (black). It can be seen that when the supply temperature reaches about 76 °C (adjustable value), the

[5] Also here, quasi-stationary conditions are required. Thus, the start-up and shut-down processes have been eliminated in the calculation. Furthermore, optical losses due to certain angular dependencies of the radiation should not occur.

flow rate is regulated (increased) to maintain the desired supply temperature provided by the planned operating concept. Due to the different irradiation conditions, the north field is connected earlier to the system. Despite maximum power output being approximately the same, the orientation of the fields results in different daily yields (Table 7).

A comparison of the measured field efficiencies with the calculated desired values is presented in Fig. 10. These values are shown depending on the mean field temperature. With increasing operating temperature (Fig. 9) and radiation, the efficiency values rise in the morning. The plant is at first operated with minimum flow rate and after with adjusted flow rate (matched flow). During the adjustment of the flow rate, the measured efficiency for the south field increases from approx. 41 % to approx. 63 %. In the north field, an increase of approx. 47 % to approx. 64 % can be seen[6]. These increases are visible in Fig. 10 as surges. After that, the fields are operated with maximum flow rate. In Fig. 10, the profiles show a small increase. In these situations, a comparison between the desired and the actual values is suitable:

- relative low changes of temperature and irradiation over time in the field and this is a prerequisite for the quasi-stationary approach,
- approximately perpendicular irradiation with a low angular dependence of the optical losses,
- high flow rate of the field with a particular flow distribution in the meander pipes (see above), with a relatively high heat transfer in the absorber pipe and with a good venting.

These statements support the comparison of the desired and actual values in Fig. 10 (north field from 11:10 to 13:10, south field from 12:20 to 14:20, CEST). The measured values (point cloud) have a slightly steeper rise compared to the calculated values. Fig. 10 also shows that the calculated collector efficiency according to Eq. 2 (green) lies in the range above the measured efficiencies (blue). The inclusion of the safety factors in Eq. 5 corrects the calculation values. The measured values of both fields are above the desired values of task 45. Therefore, the guaranteed conditions are met.

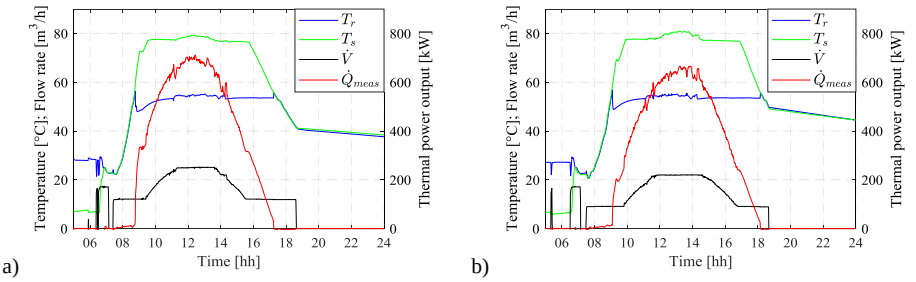

Fig. 9. Measurement results for a) the north field and b) the south field, test day 18.04.2018

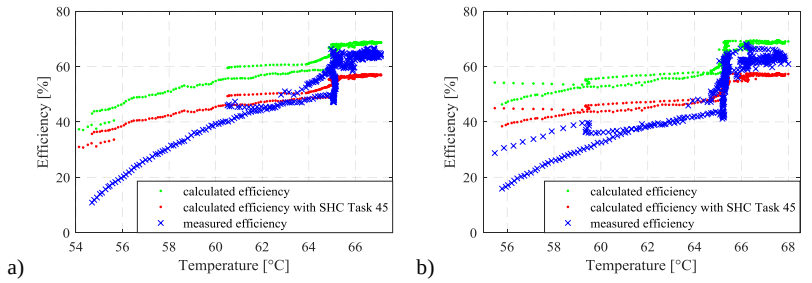

Fig. 10. Field efficiencies (Eq. 2, Eq. 6, Eq.4) depending on the mean field temperature, a) north field, b) south field, test day 18.04.2018

[6] The measured efficiencies are partly below the calculated values. The following effects are responsible for this tendency: limited capacitive effects, higher optical losses due to slanted solar radiation, relatively low flow rate with a poor heat transfer in the meander pipes.

Table 7. Overview of the investigated data for the test days 19.06.2017 and 18.04.2018

	19.06.2017		18.04.2018	
	North field	South field	North field	South field
$G_{g,Max}$ [W/m²]	995,80	994,60	1010,7	1029,7
H_g [kWh/m²]	8,07	8,05	7,31	7,62
Q_d [kWh/m²]	4,15	4,20	3,63	3,80
$\eta_{coll,meas,m}$ (actual value) [%]	64,11	64,33	63,69	63,63
$\eta_{coll,cal,m}$ (desired value) [%]	68,45	69,15	68,31	68,93
$\eta_{coll,SHCT45,m}$ (desired value) [%]	56,84	57,35	56,65	57,16
Mean temp. diff. to the ambient [%]	44,68	44,13	44,60	45,70

5. Conclusions

Two large collector fields were investigated in terms of thermal and hydraulic behavior. The fields consist of differently sized rows which are hydraulically balanced. A large number of collectors with a dividing manifold (below) and a combining manifold (above) were connected to relatively large rows.

For large collector fields, a well-chosen number of meander pipes and good setting of the regulating valve in each collector row seems to be a reliable solution to achieve a uniform flow distribution. The results show that the desired values of the efficiencies, calculated according to the SHC Task 45, can be achieved.

The operation with variable flow rate works as planned. In normal operation[7], water is suitable excellently because various properties (e.g. viscosity, density) are significantly better compared to glycol-water mixtures. The results and interrelations shown here can be transferred to other solar district heating systems. The consistently positive results confirm the concept, i.e. the construction of large rows with the selected flat plate collector and the operation.

Acknowledgements

The project underlying this report is funded by the German Federal Ministry for Economic Affairs and Energy under the code 0325871 following a decision by the German parliament. Special thanks also go to the Project Management Jülich for supporting the project. The sole responsibility for the report's contents lies with the authors.

References

[1] Urbaneck, T. et al. http://www.solfw.de. Project website, April 2018.
[2] Urbaneck, T., Oppelt, T., Platzer, B., Frey, H., Uhlig, U., Göschel, T., Zimmermann, D., Rabe, D. "Solar District Heating in East Germany – Transformation in a Cogeneration Dominated City." *Energy Procedia*, Vol. 70 (2015): 587–594. DOI: 10.1016/j.egypro.2015.02.090.
[3] Urbaneck, T., Oppelt, T., Shrestha, N. Lal, Platzer, B., Göschel, T., Uhlig, U., Frey, H. "Technische Umsetzung der solaren Fernwärme Brühl." EuroHeat&Power, VWEW Energieverlag 46. Jg. Vol 11, (2017): 20-23. – ISSN 0949-166X.
[4] Heller, A., Dahm, J. "The Marstal Central Solar Heating Plant: Design and Evaluation." *ISES Solar World Congress*, Israel, (1999): 180-187.
[5] Bava, F., Dragsted, J., Furbo, S. "A numerical model to evaluate the flow distribution in a large solar collector field." Sol. Energy 143 (2017): 31-42. DOI: 10.1016/j.solener.2016.12.029.
[6] Ohnewein, P. et al. "Hydraulikdesign von parallelen Kollektormodulen in solarthermischen Großanlagen." Endbericht Parasol, 2015.
[7] Wagner Solar. http://www.wagner-solar.com/de. April 2018.
[8] Eismann, R. "Thermohydraulische Dimensionierung von Solaranlage." Wiesbaden: Springer Fachmedien Wiesbaden GmbH, (2017): 67-70.
[9] Urbaneck, T., Schirmer, U. "Großanlage mit Vakuumröhrenkollektoren – Eine Leistungsbestimmung." 12. Symposium „Thermische Solarenergie. "Staffelstein, Ostbayerisches Technologie Transfer Institut e.V. (OTTI), Regensburg (Hrsg.), Conference Proceedings, (2016): 183-189. – ISBN 3-934681-20-4.
[10] Nielsen, J. E., Daniel, T. "Guaranteed power output. IEA Solar Heating and Cooling Programme, Task 45 Large Systems." 2016.
[11] TÜV Rheinland - DIN CERTCO, Summery of EN 12975 Test Results annex to Solar KEYMARK Certificate, DIN CERTCO, Berlin, 2015.

[7] The work in the field of active antifreeze is planned and not part of this article.